# An Orientation Inference Framework for Surface Reconstruction from Unorganized Point Clouds

Yi-Ling Chen, *Student Member, IEEE,* and Shang-Hong Lai*, *Member, IEEE*

***Abstract*—In this paper, we present an orientation inference framework for reconstructing implicit surfaces from unoriented point clouds. The proposed method starts from building a surface approximation hierarchy comprising of a set of unoriented local surfaces, which are represented as a weighted combination of radial basis functions. We formulate the determination of the globally consistent orientation as a graph optimization problem by treating the local implicit patches as nodes. An energy function is defined to penalize inconsistent orientation changes by checking the sign consistency between neighboring local surfaces. An optimal labeling of the graph nodes indicating the orientation of each local surface can thus be obtained by minimizing the total energy defined on the graph. The local inference results are propagated over the model in a front-propagation fashion to obtain the global solution. The reconstructed surfaces are consolidated by a simple and effective inspection procedure to locate the erroneously fitted local surfaces. A progressive reconstruction algorithm that iteratively includes more oriented points to improve the fitting accuracy and efficiently updates the RBF coefficients is proposed. We demonstrate the performance of the proposed method by showing the surface reconstruction results on some real-world 3D data sets with comparison to those by using the previous methods.**

***Index Terms*—Surface reconstruction, graph optimization, belief propagation, orientation inference, implicit surface.**

## I. Introduction

SURFACE reconstruction from point clouds is motivated by a number of computer-aided geometric design, point-based graphics, computer vision and scientific visualization applications due to the wide availability of point-cloud data, which may be obtained from modern laser scanners [1] or image-based techniques [2]–[8]. Among most of the existing methods, orientation information is essential during the reconstruction process and directly affects the quality of the approximation of the output surfaces [9]–[12]. While a number of existing surface reconstruction methods are capable of producing satisfactory results in terms of efficiency and quality from oriented points (i.e. each 3D data point is associated with its normal vector), less attention has been devoted to reconstruct surfaces from unoriented data sets.

In this paper, we introduce a general framework to determine the orientations of *surface primitives* derived from an unoriented point set. Traditional methods for deriving orientation information from unorganized points take the strategy of firstly estimating an unoriented normal field and then trying to propagate the orientation of a seed point over the model to align the individual normal vectors consistently [13]–[17]. These methods are designed based on the assumption that the orientations of surface normals vary smoothly between neighboring sample points. However, reliable surface normal estimation is a challenging task due to the noise embedded in the input point clouds. Furthermore, the orientation of neighboring sample points may undergo abrupt change due to non-uniformity or sparse sampling density. Therefore, orientation propagation is usually vulnerable when aligning normal vectors across sharp features or close-by surface patches. Instead of handling *discretely* sampled points, the proposed method aims to orientate a set of *continuously* defined local implicit functions (i.e. surface primitives), which better complies with the orientation consistency condition of surface primitives in a proximity and also accomplishes surface reconstruction at the same time.

The proposed method is inspired by traditional computer vision problems, e.g. stereo matching or optical flow. The famous *cooperative* stereo algorithm introduced by Marr and Poggio [18] made two basic and important assumptions followed by numerous researchers. We observe the conventional framework can also be applied when considering the orientations of surface primitives of 3D geometric models. 1) *Uniqueness*: the orientation of each surface primitive is uniquely defined with respect to the entire surface model. 2) *Continuity*: the orientations of neighboring surface primitives vary smoothly in a model. We thus formulate the determination of orientation as labeling Markov Random Fields (MRFs) with the unoriented surface primitives treated as nodes. To infer the globally consistent orientation of each surface primitive with respect to the entire model, we construct a graph connecting surface primitives in proximity and define an energy function that penalizes the inconsistent orientation change between the individual surface primitives. The tree-based orientation propagation methods [13]–[17] are similar to the proposed method from the aspect of graph labeling. Unlike previous methods that label each node in a tree by simply considering the orientation of the last visited node, we employ a probabilistic graphical model and the probability inference algorithm, i.e. belief propagation (BP) [19], to obtain an optimal labeling by minimizing the associated energy function defined on the graph.

Starting from the raw input data points that lack inherent structure and orientation information, the proposed method builds a surface approximation hierarchy comprising of a set of *unoriented* local implicit patches, which is similar to the



The authors are with the Department of Computer Science, National Tsing Hua University, Hsinchu, Taiwan. Tel: +886-3-574-2958. Fax: +886-3-572-3694. Email: {yilin,lai}@cs.nthu.edu.tw.

*partition-of-unity* approaches [20]–[23]. In addition, we adopt the *variational implicit surface* [24] represented in the form of a weighted combination of radial basis functions (RBFs) as the underlying surface representation. Unlike the previous methods that take advantages of surface normals to orientate the local surfaces, the orientations of the surface primitives are resolved through graph optimization by exploiting the *sign consistency* between neighboring surface primitives. Moreover, we further exploits the orientation consistency condition to effectively detect the erroneously fitted local surfaces. The surface primitives given a label indicating their orientations are reliably reconstructed if the local surfaces match each other in the overlapped regions with consistent orientation. The reliably fitted local surface can thus provide additional orientation information to guide the fitting process of incorrectly fitted local surfaces. A novel progressive reconstruction algorithm is introduced to iteratively improve the fitting accuracy by including more oriented data points in the surface fitting process.

The main contributions of this paper can be summarized as follows:

- An orientation inference algorithm that enables a set of surface primitives to cooperatively determine the globally consistent orientation.
- A novel progressive reconstruction algorithm suitable for variational implicit surfaces that efficiently updates the RBF coefficients by using the Schur complement formula.
- A simple and effective method for the detection and recovery of erroneously fitted local surfaces.

The remainder of this paper is organized as follows: We firstly review the related work of surface representation and reconstruction in Section II. Then, we give an overview of our approach in Section III. In Section IV, we introduce the mathematical framework of labeling unoriented surface primitives. A progressive reconstruction algorithm for RBF-based implicit surfaces is presented in Section V. Experimental results on both scanned and image-based 3D data sets with comparison to existing methods are demonstrated in Section VI.

## II. Previous Work

The literature on surface reconstruction and shape modeling is vast and a comprehensive survey is beyond the scope of this paper. Roughly speaking, most existing reconstruction algorithms can be classified into two main categories, i.e. the *parametric* and *implicit* approaches. Parametric methods usually exploit structures, such as *Delaunay tetrahedralization*, derived from computational geometry to extract a triangulated surface for an input point set. Some examples include the Alpha Shapes [25], the Power Crust algorithm [26] and the Cocone algorithm [27], [28]. The interested readers are referred to [29] for a survey. One drawback of Delaunay-based methods is that the reconstructed surfaces are interpolatory and thus inadequate to deal with noise embedded in the input point sets. On the other hand, the implicit approaches aim to find an implicit function that best fits the data by using algebraic surfaces [20], [30], [31], level set method [32], moving least squares fitting [12], [33]–[35], variational implicit surfaces using radial basis functions (RBFs) [23], [24], [36], [37], or Poisson fields [38] etc. Most of these methods require accurate and consistently oriented normals to work correctly.

To estimate the orientation of the reconstructed surface is a common problem encountered during the surface reconstruction process. Take implicit surface modeling for example. It is usually necessary to resolve the *inside/outside* ambiguity of the derived implicit functions or *signed distance fields* if there is no orientation information available, e.g. surface normals [13], [39], [40]. For Delaunay-based parametric models, the output surfaces are usually orientated by the labeling of *Voronoi poles* [41], [42]. To obtain an accurate oriented normal field is the first step in many surface reconstruction algorithms. Surface normal estimation from an unorganized point set has received considerable attention in the past [13], [16], [43]–[45]. However, the estimated normal vectors are usually ambiguously directed toward inside or outside region of the surface to be modeled. To overcome this problem, Hoppe et al. [13] proposed an orientation propagation algorithm that aligns the estimated surface normals by traversing a minimal spanning tree constructed over the data set and many variants have been developed [14], [15], [17]. In [14], an incremental algorithm was proposed to encourage the propagation front to advance in flat regions with higher priority to improve the robustness of orientation propagation. In [17], an improved preprocessing stage [46] was introduced to denoise the input point sets, remove outliers and alleviate data non-uniformities before orientation propagation. In [39], a Voronoi-based algorithm was introduced to solve a generalized eigenvalue problem for an implicit function that best fits an unoriented normal field. In [40], an active contour-based method was proposed to partition a volumetric grid into several "mono-oriented regions" followed by performing a voting procedure to decide a consistent orientation for each local surface. It is not adaptive to feature size and computationally expensive. In [47], a fast tagging algorithm was proposed to label the corners of a volumetric grid as exterior or interior so as to define the resulting surfaces.

## III. Algorithm Overview

Fig. 1 depicts the block diagram and a typical reconstruction flow of the proposed method. In our system, the reconstruction process is driven by adaptive octree subdivision. Initially, the input point set $\mathscr{P}$ is inserted into an unit bounding box, and then partitioned into a collection of overlapping subsets $\mathscr{P}_1, \mathscr{P}_2, \ldots, \mathscr{P}_M$ of low complexity, where $M$ is the number of the local subsets of $\mathscr{P}$. A local implicit function $f_i$ represented as a weighted combination of radial basis functions is fitted to approximate $\mathscr{P}_i$. An *orientation inference* stage (explained in Section IV-A) following the local surface fitting process is performed to assign each $f_i$ a label indicating the globally consistent orientation through graph optimization. To this end, an advancing front algorithm (explained in Section IV-B) is applied to iteratively propagate the partially resolved orientation assignment over the model to obtain the global solution. The consistently orientated local implicit patches

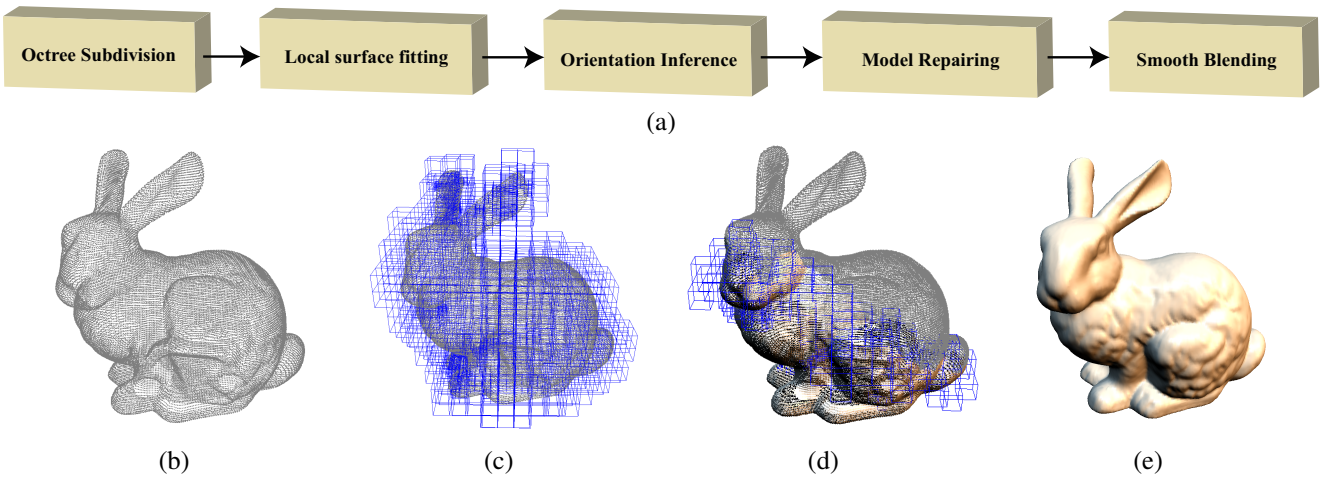


Fig. 1. (a) Block diagram of the proposed method. (b)-(e) Illustration of the typical reconstruction process of the proposed method. From left to right: The reconstruction algorithm accepts an unorganized point cloud $\mathscr{P}$ as input. Adaptive octree subdivision is performed on $\mathscr{P}$ and local surface fitting is carried out for each octree cell. An orientation inference algorithm based on graph optimization is performed to orientate the local surfaces in a front-propagation fashion. The overall implicit surface is generated by smoothly blending the orientated implicit patches.

are then smoothly blended to form the overall approximate surface.

The model repairing process is an optional stage not shown through Fig. 1(b) to 1(e), and it is usually not required when dealing with clean data sets. The objective of the model repairing stage is to take advantage of orientation consistency condition to further consolidate the fitting accuracy of the oriented local surfaces obtained from the previous orientation inference stage. To fit point sets containing complex topology or data imperfections, e.g. holes and non-uniformities, is not reliable especially when the orientation information is not provided. We thus propose a novel progressive reconstruction method that iteratively refines the local variational implicit patches by including more oriented data points from reliably reconstructed regions to guide the surface fitting process (explained in Section V).

## IV. Globally Consistent Orientation Inference

In this section we describe the mathematical framework for performing *orientation inference* on properly defined graphical models. The objective of orientation inference is to infer the *globally consistent orientation* with respect to the entire surface for each surface primitive, as pointed out in [13]. Note that implicit surfaces are typically defined as a real-valued function $f$ whose orientation is implicitly indicated by the *sign* of the evaluated values. Given a set of unoriented local shape functions $f_i$ fitted to $\mathscr{P}_i$, the goal of global consistent orientation inference is to determine a label $\ell_i$ for each $f_i$ to indicate its orientation such that the reconstructed implicit surface $f'$, which is blended by $f_i$, is consistently signed with $f$.

### A. Graph Optimization

To determine the orientation of each surface primitive is a binary optimization problem since the orientation typically reveals the *interior/exterior* part of the surface with respect to the primitive itself. The general problem we consider can thus be defined as follows. Given a geometric model that consists of a number of unoriented surface primitives. Construct an undirected graph $\mathscr{G} = (\mathscr{V}, \mathscr{E})$, with each node in $\mathscr{V}$ corresponding to one of the surface primitives and each edge in $\mathscr{E}$ indicating the connectivity of neighboring nodes. We aim to find a label $\ell_i \in \{-1, 1\}$ for each node $i \in \mathscr{V}$ such that all the surface primitives are consistently orientated. The optimal label assignment $\mathscr{L}^*$, i.e. the globally consistent orientation, is obtained through minimizing the following energy function defined on $\mathscr{G}$:

$$E(\mathscr{L}) = \sum_{i \in \mathscr{V}} E_1(\ell_i) + \sum_{(i,j) \in \mathscr{E}} E_2(\ell_i, \ell_j), \tag{1}$$

The energy function $E(\mathscr{L})$ is the sum of two terms: *singleton energy* $E_1$ and *pairwise energy* $E_2$. The singleton energy $E_1$ typically measures how well the candidate labels fit to our prior knowledge about the surface model. For the most general case, we assume that no orientation information is available and set the singleton energy to be just the sum of the negated label of node $i$.

$$E_1(\ell_i) = -\ell_i,$$

With this definition, the singleton energy $E_1$ acts as an additional constraint that selects one of the *two* optimal label assignments with more nodes labeled as 1. Note that the globally consistent orientation can be defined by assigning the label to either 1 or $-1$ for aligning the orientations of the local surface primitives. In certain applications, such as Structure from Motion (SfM), additional information (e.g. visibility through a certain line-of-sight) may be taken into account to help orientate the reconstructed data points. The pairwise energy $E_2$ captures the interaction between neighboring nodes and enables the surface primitives to cooperatively determine the globally consistent orientation. To this end, the pairwise energy should be designed to encode the *orientation consistency* between neighboring primitives.

Recall that the proposed method builds a surface approximation hierarchy by partitioning the input point set $\mathscr{P}$ through octree subdivision. Each octree cell $C_i$ has a spherical support

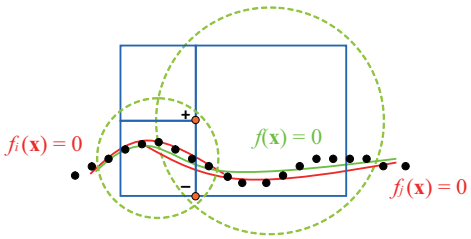


Fig. 2. The local shape functions $f_i$ and $f_j$ (red curves) are supposed to be consistently signed at the common corners (orange circles) of the octree cells where they are defined.

region that overlaps with those of neighboring cells, and a local implicit surface $f_i$ is fitted to the points in $\mathscr{P}_i$ which is contained in $C_i$. The main observation we exploit is that local implicit surfaces $f_i$ resemble the underlying surface $f$ within their support regions. Therefore, local surfaces that are geometrically adjacent to one another should be consistently signed in *most* of their overlapped support region so as to be compliant with the orientation of $f$, as illustrated in Fig. 2. The exception arises from a small margin where two neighboring local surfaces $f_i$ and $f_j$ take opposite signs due to the inevitable mismatch of shape between them. We thus define the pairwise energy as follows.

$$E_2(\ell_i,\ \ell_j) = \sum_k -\ell_i \cdot \ell_j \cdot sign(f_i(\mathbf{x}_k) \cdot f_j(\mathbf{x}_k)), \tag{2}$$

where $k$ is the index of the *auxiliary points* for checking the sign consistency, and $sign(\cdot)$ is a binary function that returns 1 or $-1$ when its argument is positive or negative, respectively. By evaluating $sign(f_i(\mathbf{x}_k) \cdot f_j(\mathbf{x}_k))$, a returned value 1 indicates that $f_i$ and $f_j$ have consistent orientation at $\mathbf{x}_k$, otherwise they are inconsistent. As a result, $E_2(\ell_i,\ \ell_j)$ penalizes the inconsistent orientation change of two neighboring local surfaces $f_i$ and $f_j$. Note that the positions of auxiliary points should be important for sign checks and we have chosen the common corners shared by two adjacent octree cells $C_i$ and $C_j$. Denote $k$-connected neighbors of a cell $C_i$ as those adjacent cells of $C_i$ that share $k$ common corners with $C_i$. For robustness, we only include 4-connected neighbors, which provides the most common corners shared with each other, into graph optimization. By taking advantage of the connectivity in the octree hierarchy, the local surfaces corresponding to adjacent cells are enabled to cooperatively determine the optimal orientation assignment by setting up an energy function as Equation (1) for minimization.

To find the optimal labeling $\mathscr{L}^*$ that yields the least cost of $E(\mathscr{L})$ corresponds to the *maximum a posteriori* (MAP) estimation problem on $\mathscr{G}$. The MRF labeling problem has been recognized to be computationally difficult, especially when the number of possible labels and the size of the graph are large. In our case, the optimization problem formulated above can be efficiently solved by the fast inference algorithms, such as *graph cuts* [48] and *belief propagation* [19]. We have chosen the belief propagation algorithm to optimize the MRF labeling problem because it may benefit from faster convergence by exploiting the previous results for message passing during the process of the advancing-front algorithm, which will be explained in the next subsection.

In a sense, the graph $\mathscr{G}$ can be regarded as a joint probability of a set of binary random variables with the edges indicating the dependency between distinct nodes. Belief propagation works by iteratively propagating *messages* or *beliefs* along edges over a graph. Let us denote the message sent from node $i$ to $j$ as $m_{i\to j}$. In our formulation, message $m_{i\to j}$ is a two-dimensional vector, and can be regarded as the probability density function that node $j$ takes label 1 or $-1$. During each iteration, each node receives and updates its message by forming product of incoming messages and local evidence as the following equation:

$$m_{i\to j}(\ell_j) = Z \max_{\ell_j}(E_1(\ell_i) \cdot E_2(\ell_i,\ \ell_j) \cdot \prod_{u \in Nbhd(i)\setminus j} m_{u\to i}(\ell_i)), \tag{3}$$

where $Nbhd(i)\setminus j$ denotes the neighbors of $i$ other than $j$, and $Z$ is a normalization factor. Finally, the MAP solution for each node $i$ is computed as

$$\ell_i^* = Z \max_{\ell_i}(E_d(\ell_i) \cdot \prod_{u \in Nbhd(i)} m_{u\to i}(\ell_i)), \tag{4}$$

For tree structured graphs, BP is guaranteed to converge to a fixed message $m^*$ after at most $T$ iterations depending on the longest path of the graph. For graphs with loops, Loopy BP [49] can be applied to obtain good approximate solutions. The BP algorithm comes with two variants: *sum-product* and *max-product*. In this paper, we use the max-product algorithm to find a MAP solution to the graph optimization problem formulated earlier in this section by taking negative log probabilities.

### B. Advancing-Front Algorithm

Intuitively, to obtain the optimal label assignment, a global graph consisting of all the surface primitives should be constructed for the energy minimization procedure. However, we choose to infer the orientations locally and iteratively propagate the partially determined results over the entire model to obtain the global solution due to the following two observations:

1) The interaction between the signed distance functions associated with adjacent surface primitives is essentially a local property. That is the reason why we construct a graph that encodes the adjacency relationship.
2) Previous results provide additional information for further inference.

Therefore, we devise the advancing-front algorithm outlined in Algorithm 1. Initially, we have a collection of octree cells $C_i$ with corresponding unoriented local implicit surfaces $f_i$. Starting from a *seed* cell, the algorithm proceeds by iteratively marching an active octree cell $C_{active}$ to traverse the unchecked regions of the model until all the local implicit surfaces have been properly orientated. During the process of traversal, each cell may be assigned to one of the following three possible lists: `unchecked`, `active` and `checked`. Conceptually, all the local surfaces are marked as unchecked in the beginning and the `active` list contains only the seed cell. In each

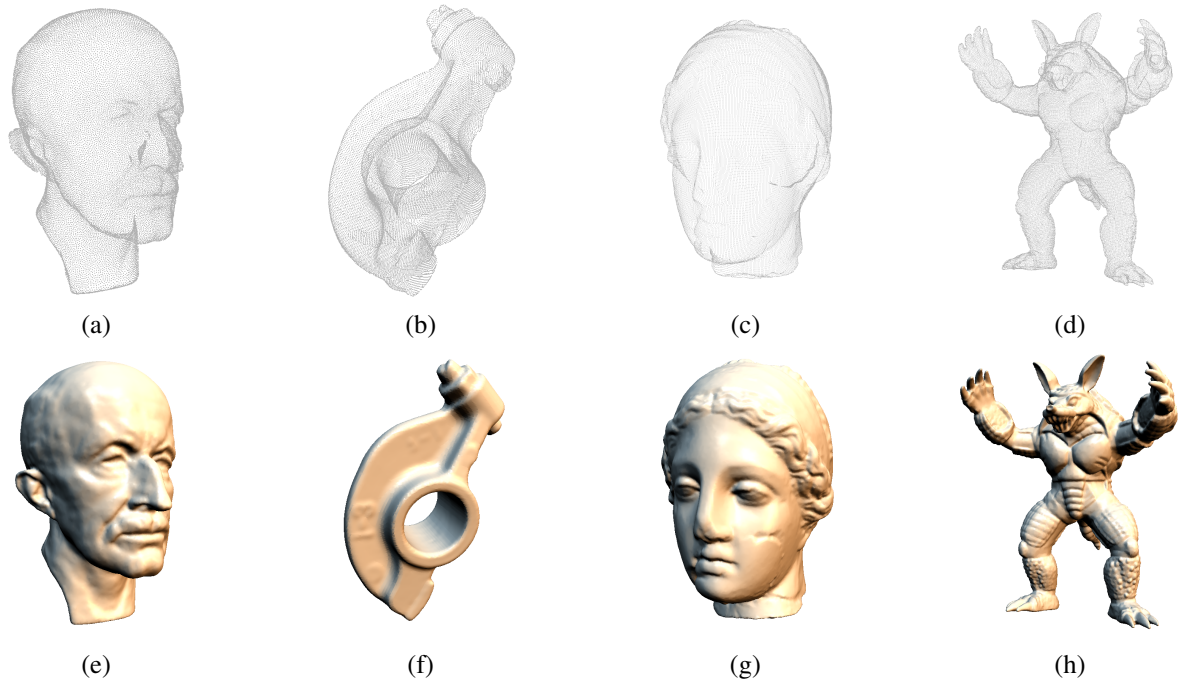

Fig. 3. (a)-(d) Input raw point sets rendered with the surface normals obtained by the proposed method. (e)-(h) Reconstructed implicit surfaces by the proposed method.

**Algorithm 1** OrientationPropagate($F$ = null)

```
Select seed cell v and insert v into F.
while F not empty do
  C_active = F.front;
  Construct graph G with C_active;
  Perform BP inference on G;
  Update labels of the nodes in G;
  Find and insert adjacent cells of G into F;
end while
return
```

iteration, the first cell of the `active` list is selected to build a local graph $\mathscr{G}$. The graph construction procedure can be briefly summarized as follows: starting from an active cell $C_{active}$ as a node of $\mathscr{G}$, we search the `unchecked` list for the 4-connected neighbors of $C_{active}$ and link $C_{active}$ with them. The same procedure is repeatedly applied to the newly added graph nodes until at least one checked cell has been included into $\mathscr{G}$. The cells adjacent to a graph node are activated and inserted into the `active` list. As a result, the `active` list behaves like a frontier which advances toward the unchecked regions of the model. After applying the BP inference algorithm to $\mathscr{G}$, the labeled cells are moved to `checked` list, which ends a single iteration of Algorithm 1. In practice, each cell can be associated with a tag indicating its status and the connectivity between cells can be efficiently queried with the octree hierarchy. Therefore, only the `active` list or *front* $F$, which contains a queue of candidate cells to be selected for the orientation inference process in the next iteration, needs to be explicitly maintained. To summarize, the basic idea of this incremental algorithm is straightforward: traversing all the leaves among the octree in the order of connected components of visited cells. The belief propagation inference is performed on a graph constructed subject to the active cell. The advancing front $F$ will roughly trace along the locus of the underlying surface until it becomes empty.

## V. Progressive Reconstruction of Variational Implicit Surfaces

To establish a *progressive* or *multi-scale* representation of implicit surfaces is attractive when the complexity of geometric models is very high in terms of data size or topology. Such models are expensive to store, transmit and render. A multi-scale implicit surface representation enables the control of level-of-detail by using the most significant data points to reconstruct the underlying surface. A coarse surface can then be refined by progressively adding additional data points. However, because of the global support nature of radial basis functions, adding only a few new data points leads to complete re-computation of the resulting RBF coefficients. Using compactly supported RBFs [23], [50] leads to more efficient computation, which involves in a sparser matrix. However, it has the drawback that sparsely or irregularly sampled regions may not be interpolated or fitted well. In this section, we introduce an algebraic solution to alleviate the high computational cost of progressively reconstructing RBF-based implicit surfaces by using the Schur Complement formula [51] and further apply it for *model repairing*.

### A. Schur Complement Formula

Before introducing the proposed progressive reconstruction algorithm, let us firstly reconsider the scattered data interpolation problem by variational techniques [24], [52]. Given a set of $N$ constraint points $\mathscr{P} = \{\mathbf{x}_1, \mathbf{x}_2, \ldots, \mathbf{x}_N\}$ that are scattered

on or near the unknown surface with the corresponding scalar height fields $h_1,\ h_2,\ \ldots,\ h_N$, find $f$ that satisfies the interpolation conditions: $f(\mathbf{x}_i) = h_i,\ i = 1,\ 2,\ \ldots,\ N$. Expressing the interpolant function $f$ as a weighted combination of RBFs in Equation (5) leads to the smoothest function among all possible solution functions with minimum aggregate curvature:

$$f(\mathbf{x}) = \sum_{j=1}^{N} w_j \phi(\mathbf{x} - \mathbf{x}_j) + p(\mathbf{x}), \tag{5}$$

where $\mathbf{x}_j = (x_j,\ y_j,\ z_j)$ are the locations of the constraints, $w_j$ are the weights, and $p(\mathbf{x})$ is a first-degree polynomial accounting for the linear and constant term of $f$. There is a rich variety of radial basis functions suggested in the literature. For 3D interpolation, we adopt the pseudo-cubic basis function $\phi(r) = r^3$, as used in [24], [52]. Solving for the unknowns, $w_1,\ w_2,\ \ldots,\ w_N$, and the coefficients of $p(\mathbf{x})$, in the interpolation function $f$ leads to solving the following linear system:

$$\begin{pmatrix} A & P \\ P^T & O \end{pmatrix} \begin{pmatrix} w \\ \lambda \end{pmatrix} = \begin{pmatrix} h \\ 0 \end{pmatrix}, \tag{6}$$

where $A_{ij} = \phi(\|\mathbf{x}_i - \mathbf{x}_j\|)$. The polynomial part of the interpolation function $f$ in Eq. (5) has the form of $p(\mathbf{x}) = \lambda_0 + \lambda_1 x + \lambda_2 y + \lambda_3 z$, and thus $P$ is the matrix with the $i$-th row being $(1, x_i, y_i, z_i)$. Note that the sub-matrix $A$ is positive-definite and the solution to Eq. (6) can be easily solved by direct methods, such as LU decomposition or singular value decomposition (SVD). Typically, the scalar values $h$ corresponding to the data points where the implicit surface passes through are set to zero and some *off-surface constraints* inside or outside the surface are created by extending the *on-surface constraints* along the directions of surface normals for a certain distance [24]. It is worth noting that initially we cannot obtain correctly orientated local surfaces because the off-surface constraints required to determine the orientation cannot be explicitly specified in absence of real surface normals. Orientation inference is thus applied to resolve the orientations of the local surfaces.

To achieve progressive reconstruction, additional constraint points are repeatedly appended to the linear system of (6) and the corresponding RBF coefficients need to be updated. Since the linear system is getting larger, directly applying LU decomposition or SVD requires $O(N^3)$ computational complexity to re-compute the RBF coefficients, which is quite computationally expensive especially when $N$ is large. In this paper, we propose an algebraic approach to alleviate the cost of iteratively updating globally supported radial weights by using the Schur complement formula [51]. Schur complement formula gives the closed-form expression for the inverse of a partitioned matrix. Firstly, we rearrange the linear system in Equation (6) as below:

$$\begin{pmatrix} O & P^T \\ P & A \end{pmatrix} \begin{pmatrix} \lambda \\ w \end{pmatrix} = \begin{pmatrix} 0 \\ h \end{pmatrix}, \tag{7}$$

During the process of progressive reconstruction, the matrix of our progressive reconstruction problem can thus be expressed by the following $2 \times 2$ partitioned matrix:

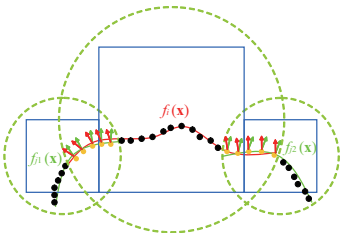


Fig. 4. Detection of vulnerable cells by performing an additional orientation consistency check on the overlapped support regions between neighboring local surfaces.

$$K = \begin{pmatrix} K_{11} & K_{12} \\ K_{21} & K_{22} \end{pmatrix}, \tag{8}$$

where $K_{11}$ is the matrix in Eq. (7) formed by the existing RBF centers. The sub-matrix $K_{12} = K_{21}^T$ contains the interaction between the newly added centers and existing centers. $K_{22}$ is a square matrix corresponding to the newly added centers. To update the old coefficients and solve for the new ones, we need to solve the linear system $K\mathbf{w} = \mathbf{h}$. According to Schur complement formula, the inverse matrix $K^{-1}$ can be written in the following form:

$$K^{-1} = \begin{pmatrix} K_{11}^{-1} + K_{11}^{-1} K_{12} S^{-1} K_{21} K_{11}^{-1} & -K_{11}^{-1} K_{12} S^{-1} \\ -S^{-1} K_{21} K_{11}^{-1} & S^{-1} \end{pmatrix}, \tag{9}$$

where

$$S = K_{22} - K_{21} K_{11}^{-1} K_{12},$$

Compared with solving the whole linear system with the direct methods of $O(N^3)$ complexity, the computation of $K^{-1}$ using the Schur complement formula involves only multiplication of the partitioned matrices with $K_{11}^{-1}$ and $S^{-1}$. Note that $K_{11}^{-1}$, which is the inverse matrix corresponding to the old RBF coefficients, is computed and stored in the previous iteration. The size of the matrix $S$ depends on the number of newly added RBF centers and it is usually quite small compared to the size $K_{11}$. By storing $K_{11}^{-1}$, we can exploit the Schur Complement formula to solve the new linear system with low cost. In the aspect of time complexity, we can focus on the analysis of $K_{11}^{-1} K_{12} S^{-1} K_{21} K_{11}^{-1}$, which involves in the most intensive computation in Eq. (9). It includes a series of matrix multiplication. Let us denote the numbers of original and newly added constraints as $N$ and $p$, respectively, and assume that $p$ is much less than $N$. Since the complexity of multiplying $m \times p$ and $p \times n$ matrices is $O(mnp)$, the complexity of computing the above block matrices is bounded to $O(N^2 p)$. Obviously, it is most advantageous to exploit Schur Complement formula when $p$ is small since the direct methods have the complexity of $O(M^3)$, where $M = N + p$ is the total number of constraints. Two examples of progressive surface reconstruction are given in Fig. 6 and Fig. 7.

### B. Model Repairing

Surface fitting of topologically complex local point sets $\mathscr{P}_i$ without orientation information is very challenging, especially when $\mathscr{P}_i$ is sparsely or non-uniformly sampled. Inspired by

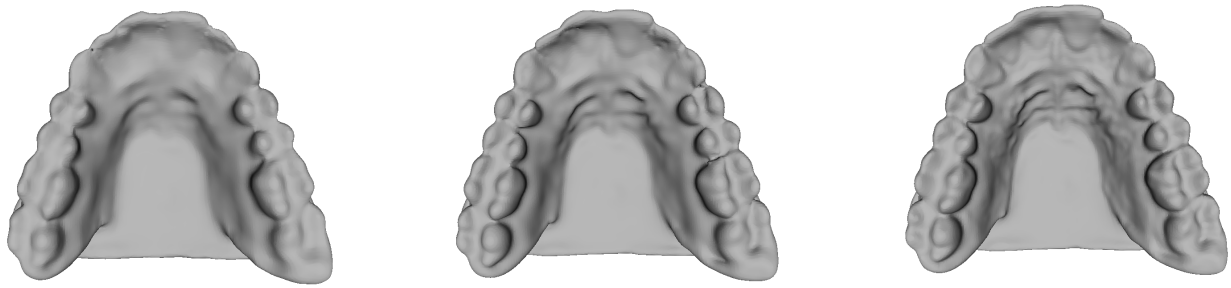

(a) (b) (c)

Fig. 6. From left to right: Coarse-to-fine reconstruction of the TEETH data set consisting of 116604 points. The numbers of RBF centers used in various resolutions of reconstructed models are 11767, 32716 and 48451, respectively. The finest model shown in (c) achieves the fitting accuracy of $3 \times 10^{-4}$ (with respect to the main diagonal of an unit bounding box).

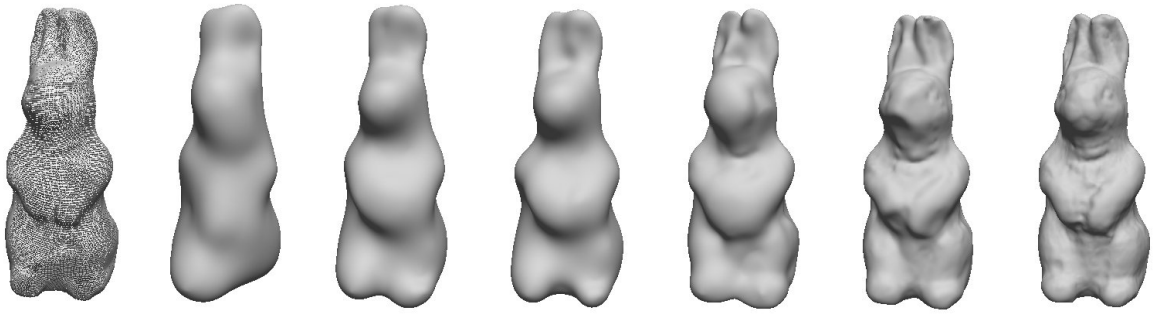

Fig. 7. Coarse-to-fine reconstruction of the RABBIT data set consisting of 67038 points under different octree levels. From left to right: The leftmost image shows the input point set. The second to fourth images show models of different resolutions reconstructed under octree level 2. The fifth to the rightmost images show models reconstructed under octree levels 3, 4 and 5, respectively. The rightmost image shows the finest model which achieves the fitting accuracy of $5 \times 10^{-4}$ (with respect to the main diagonal of an unit bounding box).

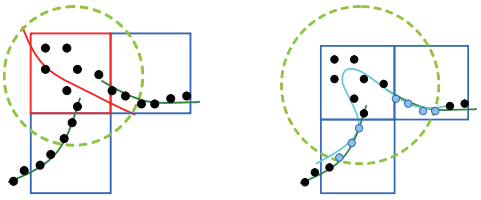

(a) (b)

Fig. 5. (a) A vulnerable cell with an erroneously fitted local surface. (b) Iteratively enlarge the support region to include more oriented points and perform model refitting.

the orientation consistency check exploited in our orientation inference algorithm, a simple and effective model repairing procedure is proposed for detecting and recovering the local surfaces that are potentially not well fitted. The basic idea is to reinforce the orientation consistency condition on each orientated local surface $f_i$ and to examine if the overlapped support regions of $f_i$ and its neighboring local surfaces $f_j$ are consistent in orientation, as illustrated in Fig. 4 with a 2D example. This additional check is effective because if $f_i$ is correctly reconstructed and orientated, it is supposed to be consistent in orientation with neighboring $f_j$ to form a continuous surface. After the orientation inference stage, we thus perform the following procedure on a local surface $f_i$ to detect and recover the potential errors:

1) Collect the point set $\mathscr{P}_i$ from the points in the data set $\mathscr{P}$ that are located within the support region of $C_i$.
2) Find the subset $\mathscr{P}_i'$ of $\mathscr{P}_i$, which also lies in the support regions of neighboring local surfaces $f_j$.
3) For each point $\mathbf{x}^k \in \mathscr{P}_i'$, evaluate the gradients of $f_i$ and $f_j$ as estimated normal vectors $\mathbf{n}_i^k$ and $\mathbf{n}_j^k$.
4) Compute $\delta_i = |\{\mathbf{x}^k | \mathbf{x}^k \in \mathscr{P}_i' \text{ and } \mathbf{n}_i^k \cdot \mathbf{n}_j^k > 0\}|/|\mathscr{P}_i'|$ to indicate the *vulnerability* of $f_i$.

The above steps compose the *detection* part of the model repairing procedure. Note that $\delta_i$ is the ratio of inconsistently oriented points among $\mathscr{P}_i'$. For those $f_i$ of high $\delta_i$, $f_i$ is potentially not well fitted. In contrast, $f_i$ of low $\delta_i$ can be regarded as reliable and is able to provide approximate normal vectors as additional information to guide the refitting of vulnerable local surfaces. We have empirically chosen a global threshold $\delta^* = 0.1$ to mark $f_i$ as vulnerable if $\delta_i$ is larger than $\delta^*$ and it works well for all of our test data sets. For each $f_i$ marked as vulnerable, we then perform the following *recovery* procedure:

1) Enlarge the support region of $f_i$ and find the corresponding constraint point set $\mathscr{P}_i''$.

2) Update the RBF coefficients of $f_i$ by using Schur Complement formula.
3) Recompute $\delta_i$. If $\delta_i > \delta^*$, go to step 1). Otherwise, terminate.

As depicted in Fig. 5, during the recovery process, we iteratively enlarge the support region of $f_i$ to include more oriented points from other reliable local surfaces $f_j$. The estimated normals from $f_j$ may help orientate $f_i$ by creating additional off-surface constraints along the normal directions during RBF fitting [24]. Since the new constraint point set $\mathscr{P}_i''$ contains the original data set $\mathscr{P}_i$ with some additional constraint points, the progressive reconstruction algorithm explained in Section V-A can be exploited to refit $f_i$ until the corresponding $\delta_i$ is less than $\delta^*$. It is worth noting that it would be difficult for the traditional orientation propagation methods [13]–[17] to perform similar correctness check after the unoriented normal vectors are aligned, because they are designed for discrete surface samples whose normal vectors occasionally violate the orientation consistency condition. Therefore, if normal directions are incorrectly aligned, the errors cannot be detected by the previous methods, then the normal direction errors will be propagated because the normal vectors are aligned in a way such that they are consistently directed with those of neighboring surface samples.

## VI. Experimental Results

To evaluate the performance of our method, we have applied it to two types of data sets of different characteristics, i.e. point sets obtained from 3D scanning and image-based 3D reconstruction [8]. All experimental results presented in this section were generated on a PC equipped with an Intel Core 2 processor at 2.93GHz and 2GB main memory. Recall that in our system the input point set $\mathscr{P}$ is partitioned into local subsets $\mathscr{P}_i$ of low complexity by octree subdivision and then RBF fitting is performed on each subset $\mathscr{P}_i$. Although the RBF-based implicit surfaces possess good data approximation ability, they are more computationally expensive to compute and evaluate when compared with other implicit representations, such as quadrics or polynomials of low degrees. Unlike other partition-of-unity approach [20] that recursively decomposes a cell until the corresponding local surface achieves a prescribed accuracy [30], we have adopted a simple but practical criterion to build the octrees by using two threshold values to guide the octree subdivision. Cell $C_i$ is partitioned whenever the number of points of $\mathscr{P}_i$ is larger than $\lambda_{high} = 100$ without RBF fitting. If $|\mathscr{P}_i|$ is less than $\lambda_{high}$, we measure how well $\mathscr{P}_i$ approximates to a disk-like region by performing local covariance analysis [53]. If $\mathscr{P}_i$ is planar, the RBF coefficients of $f_i$ are computed; otherwise $C_i$ is further decomposed. However, if $|\mathscr{P}_i|$ is less than $\lambda_{low} = 30$, the recursion of octree refinement is terminated. We set up the second threshold to ensure enough surface samples are included in the local surface fitting because further subdivision of $C_i$ does not necessarily improve surface fitting quality, especially when sparse or non-uniform sampling is common in the case of image-based data sets. We resort to the model repairing stage to consolidate the fitting accuracy and the purpose of $\lambda_{low}$ is to avoid repetitive octree refinement and model refitting.

TABLE I
Computation time (in seconds) of the proposed algorithm on some 3D scanned data sets.

| Data Set | Data Size | Octree | RBF Fitting | Orientation |
|---|---|---|---|---|
| Bunny | 35947 | 1.16 | 6.45 | 8.13 |
| RockerArm | 40177 | 0.63 | 4.32 | 4.54 |
| MaxPlanck | 49132 | 0.79 | 6.94 | 5.92 |
| Venus | 134345 | 0.89 | 19.86 | 8.89 |
| Armadillo | 172974 | 4.02 | 21.78 | 23.38 |

TABLE II
Computation time (in seconds) of the proposed algorithm on some image-based 3D data sets.

| Data Set | Data Size | RBF Fitting | Orientation | Repairing |
|---|---|---|---|---|
| Horse | 18532 | 3.14 | 4.78 | 2.36 |
| Dragon | 27048 | 4.09 | 5.02 | 2.16 |
| Dinosaur | 34116 | 4.39 | 4.69 | 4.72 |
| Ness | 51614 | 9.51 | 8.49 | 0.78 |
| Statue | 55324 | 8.31 | 7.54 | 0.33 |

### A. Scanned Data Sets

Much practical motivation of surface reconstruction derives from 3D scanning. Compared with image-based 3D reconstruction data, 3D scanned data sets are of relatively higher accuracy and are usually accompanied with orientation information, such as surface normals. Despite the advance of modern 3D scanning technology, the acquisition or estimation of orientation information is not always reliable for some situations such as specular reflections, material artifacts, and shadowing [54], [55]. Nevertheless, we have discarded all the orientation information contained in the input point sets for experiments. Computation time of applying the proposed method to several 3D scanned data sets is summarized in Table I. One can see that the proposed method performs efficiently with all the test models. Unlike the previous orientation propagation methods [13], whose complexity is proportional to the number of data points, the complexity of the proposed method is affected by the number of octree cells (or local surfaces). As a result, 3D models of large data sizes do not necessarily take more time on orientation inference because the number of local surfaces does not significantly increase due to over-sampling (take Venus as an example when compared with Bunny). On the other hand, when comparing Bunny with RockerArm and MaxPlanck of similar sizes, it obviously takes more time for the orientation estimation because the Bunny data set has relatively more complex shape, and thus requires more local surfaces. As shown in the bottom row of Fig. 3, one can see that the reconstructed implicit surfaces have been correctly orientated by examining the reconstructed models.

### B. Image-based Data Sets

The second category of data sets used in our experiment are those acquired from *Structure from Reflection* technique [8], which recovers 3D structures from multiple reflections of a real object contained in a single image (see Fig. 8 for some examples). Compared with scanned data sets, image-based

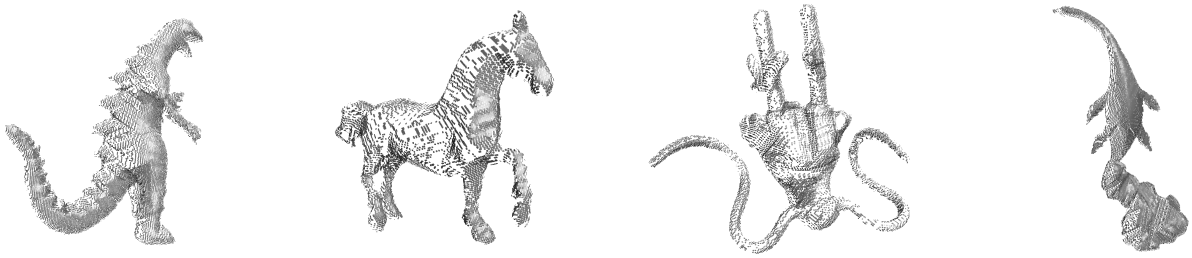

Fig. 9. Examples of the point clouds obtained by Shape from Reflection.

Fig. 8. Examples of the input images used for Shape from Reflection.

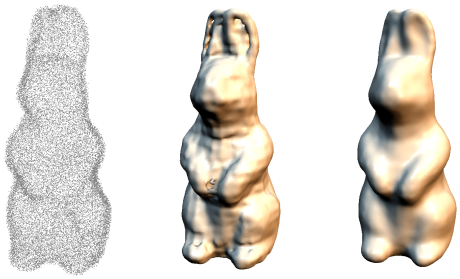

(a) (b) (c)

Fig. 10. (a) RABBIT data set perturbed with 1% random noise with respect to the size of an unit bounding box. (b) reconstructed implicit surface with regularization parameter $\lambda = 0.001$. (c) reconstructed implicit surface with regularization parameter $\lambda = 0.01$.

(a) (b)

Fig. 11. Model repairing on DINOSAUR data set. (a) Reconstructed surface without model repairing, (b) Reconstructed surface with model repairing.

data sets are inferior in terms of accuracy and commonly suffer from sparse, non-uniform sampling or holes, as illustrated in Fig. 9. To achieve better robustness of local surface fitting, a regularization parameter $\lambda$ is added to the main diagonal of the linear system in Equation 7, which causes the implicit surfaces to smoothly fit to the data points instead of exact interpolation [37]. As shown in Fig. 10 (b) and (c), the noise accompanying the input data degrades the accuracy of local surface fitting and its effect is alleviated by increasing the regularization parameter $\lambda$.

Table II summarizes the computation time of the proposed algorithm on several image-based 3D data sets. The computation time of model repairing depends on the quality of the corresponding data sets and typically composes only a small portion of the overall computation time. Fig. 11 demonstrates an example of model repairing on the DINOSAUR data set. This data set suffers from low sampling density in some regions (e.g. the paws of the dinosaur) and the corresponding local surfaces were not well fitted, leading to visible artifacts (see Fig. 11(a)). Although model repairing still cannot recover the fine features (e.g. the claws) due to insufficient data samples, the artifacts are removed because the repaired local surfaces are continuous in orientation (see Fig. 11(b)). Fig. 16 shows several models with color mapping back to the original images.

### C. Progressive Reconstruction

To demonstrate the effectiveness of the proposed progressive reconstruction algorithm, we have implemented a coarse-to-fine reconstruction procedure similar to [36]. In the beginning, RBF fitting is carried out with a coarse subset $\mathscr{P}_i'$ uniformly subsampled from each local point set $\mathscr{P}_i$. The residuals of the unused data points $\mathscr{P}_i'' = \mathscr{P}_i \setminus \mathscr{P}_i'$ are computed by evaluating the local implicit function $f_i$ fitted to $\mathscr{P}_i'$. We take the greedy strategy of appending a certain number of new RBF centers with greatest residuals to $\mathscr{P}_i'$, refitting $f_i$ and updating the residuals of the remaining data points. The above procedure is repeated until the residuals of $\mathscr{P}_i''$ are less than a prescribed fitting accuracy. Fig. 6 and 7 illustrate examples of progressively reconstructing implicit surfaces from the RABBIT and TEETH data sets consisting of 67038 and 116604 points, respectively. In Fig. 6, iterative refinement is performed on the local implicit surfaces corresponding to the leaves of the octree hierarchy. To further control the level-of-details, the refinement process can also be carried out in different levels of the octree, as shown in Fig. 7. In these examples, starting from the coarsest models, we added 5 new constraints during each refinement step and it took 3461 and 5280 iterations to obtain the finest models shown in the rightmost images of Fig. 6 and 7, respectively. In these two experiments, the progressive reconstruction by Schur complement formula reduces the RBF fitting time compared to that by using the direct methods from 40 to 26 seconds and from 51 to 32 seconds, which correspond to performance gains of 35% and 37.3%, respectively. Although the proposed

(a) (b) (c)

Fig. 12. Surface reconstruction of the NESS data set by using point consolidation [17] in conjunction with Poisson surface reconstruction [38] (a) the intermediate point cloud after applying WLOP, (b) the point clouds rendered by normal vectors after orientation propagation with back culling, (c) reconstructed surface by Poisson reconstruction.

progressive reconstruction algorithm exploiting the inverse matrix stored in the previous iteration leads to more efficient computation of the RBF coefficients, it introduces some small numerical errors due to the limited precision of floating-point arithmetic, which will be accumulated during the process of iterative refinement. In practice, we apply the direct methods to solve for RBF coefficients for every 20 iterations to eliminate the accumulated numerical errors.

### *D. Comparison with Previous Methods*

For comparison, we have chosen the state-of-the-art orientation determination method presented in [17]. The *point consolidation* algorithm consists of two main components: preprocessing based on *weighted locally optimal projection* (WLOP) operator followed by reliable normal estimation. The WLOP operator improves LOP originally developed in [46] to produce a set of denoised, outlier-free and evenly distributed particles over the original dense point cloud. The unoriented normal vectors are estimated by classical local PCA [53] and then aligned through traditional propagation scheme [13] with new priority measure to deal with challenging scenarios, such as propagation across close-by surface sheets. Since it is not a reconstruction algorithm, we input the orientated point clouds to the Poisson surface reconstruction [38] to obtain the reconstructed surfaces. The implementations are provided by the authors of the original papers.

We have conducted experiments on the more challenging image-based 3D reconstruction data sets for comparison. Fig. 12 and 13 depict some examples of the surface reconstruction results obtained by applying the point consolidation in conjunction with Poisson reconstruction. The results were generated by using the parameters automatically computed by the program except that we did not downsample the raw input as much as the default setting because the data sizes are not very large. We took the same downsampled raw point sets before applying WLOP as input to our method and the corresponding results can be found in Fig. 16. As shown in Fig. 12(a) and Fig. 13(a), the intermediate point clouds after applying WLOP are generally more uniformly distributed and less noisy. However, the following orientation propagation stage was not able to correctly resolve the orientation of the estimated normal fields. In Fig. 12(b) and Fig. 13(b), one can

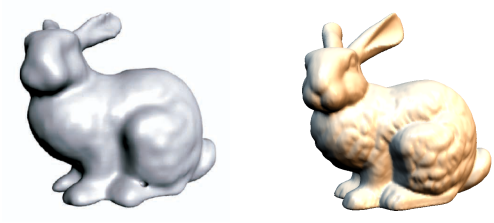

(a) (b)

Fig. 14. Reconstructed surfaces from the BUNNY data set by using (a) volumetric regularization [37], and (b) the proposed method, respectively.

observe that large parts of the normal fields were erroneously assigned to an opposite orientation (directed toward inside), and if the point clouds are rendered with back culling, the corresponding points become invisible. If the point sets with wrong normal fields are passed to the Poisson surface reconstruction algorithm [38], the reconstructed surfaces are accompanied with artifacts, as shown in Fig. 12(c) and Fig. 13(c). The proposed method deals with implicit functions instead of normal vectors and accomplishes surface reconstruction at the same time. One can see that the proposed method correctly orientates and reconstructs the implicit surfaces for all test data sets. Generally, orientation propagation is efficient but requires the overhead of preprocessing. For example, it took 14.59 seconds to obtain the intermediate result of the NESS data set shown in Fig. 12 (a) and (b). Nevertheless, our method will also benefit from some data preprocessing like WLOP, especially when outliers exist in the input point sets

The *volumetric regularization* technique is also highly related with the proposed method, which was developed to deal with image-based 3D data sets [37]. The main differences between them are that the volumetric regularization technique is a global RBF fitting method and it exploits the notion of *free space* to orientate the reconstructed implicit surfaces. The free space means the region along the line-of-sight between the camera and the object, which provides additional information of locations outside the object. A global RBF fitting method has the advantages of high tolerance to noise and hole filling. However, it also suffers from the high complexity of solving a linear system consisting of all the constraint points describing the global surface. As a result, it has been limited to several thousands of constraints and subsampling is usually necessary for large data sets. Fig. 14(a) shows the BUNNY model reconstructed by volumetric regularization [37]. Due to the limited number of constraints, much local surface detail can not be well preserved and becomes smoothed out. The proposed method accomplishes adaptive approximation which well preserves local surface detail, and orientates the local implicit surfaces without using any prior knowledge (see Fig. 14(b)).

Fig. 15 compares the *algebraic point set surfaces* (APSS) [15] with the proposed surface reconstruction method. APSS is a recently developed surface reconstruction algorithm based on moving least squares fitting of algebraic spheres instead of traditional plane fitting. It also includes an orientation propagation scheme similar to [13] with new heuristics to propagate normal orientation. The implementation of APSS

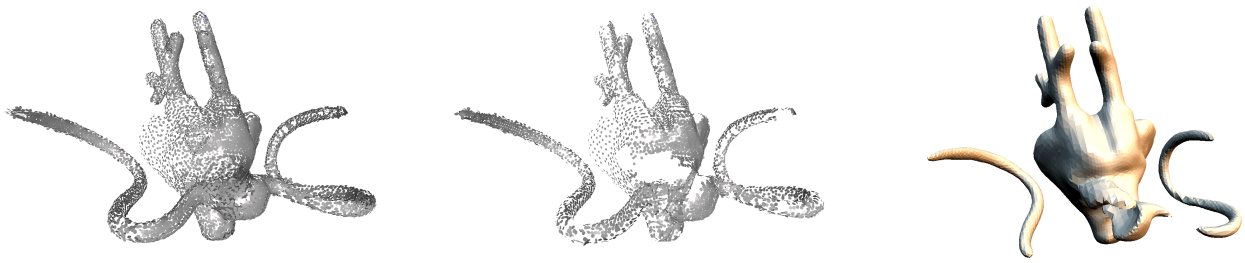

(a) (b) (c)

Fig. 13. Surface reconstruction of the DRAGON data set by using point consolidation [17] in conjunction with Poisson surface reconstruction [38] (a) the intermediate point cloud after applying WLOP, (b) the point clouds rendered by normal vectors after orientation propagation with back culling, (c) reconstructed surface by Poisson reconstruction.

is available in the open source software, MeshLab [56]. Despite its claim of high stability against undersampling, one can see that APSS still produces artifacts in some test data sets, as shown in Fig. 15 (a) and (c). In contrast, the data approximation ability of RBFs enables the proposed method to smoothly reconstruct the underlying surfaces even in the presence of data non-uniformities and holes (see Fig. 15 (b) and (d)).

## VII. DISCUSSIONS

In this section, we briefly examine the advantages and limitations of the proposed method. The basic idea of the proposed orientation inference method is to treat continuous implicit functions as unoriented primitives instead of discrete surface samples, which have been adopted by most existing methods. We resolve the orientations of these implicit primitives to enforce global orientation consistency through a graph optimization scheme, which is an advantage over the existing methods. In previous methods, many sophisticated techniques, such as priority-driven propagation, feature detection and denoising, were developed to improve the robustness of orientation propagation. However, even with these efforts, orientation propagation algorithms still fail in some difficult cases, such as data non-uniformities or sparse data sampling. The main reason is that discrete primitives are weakly compliant with or even violate the orientation consistency assumption. It is worth noting that it is possible to modify the proposed method to align an unoriented normal field by treating the individual normal vectors as primitives under the same graph optimization framework. Nevertheless, the success of such an approach also depends on whether the neighboring discrete primitives in a graph are compliant with the orientation consistency assumption or not. Therefore, continuous primitives are preferable and potentially more robust than discrete ones.

The proposed method adopts the surface representation of radial basis functions because of their good approximation ability. It is driven by octree subdivision and builds a hierarchy of local implicit surfaces, which are then orientated by the proposed cooperative framework. Compared with the global RBF fitting methods [24], [37], the proposed method achieves adaptive local approximation and possesses a certain extent of hole filling and noise tolerance. However, it will be difficult for the proposed method to handle data sets with large missing areas due to its local fitting strategy. In contrast with volumetric grid-based orientation determination methods [40], [47], the proposed method is adaptive to feature sizes. Due to the smooth interpolation nature of RBFs, the proposed method cannot well preserve sharp features presented in the models. Sharp features may be preserved by identifying the multiple surface patches that compose the features and performing piecewise surface fitting [20], [34]. However, it will need a more sophisticated orientation inference algorithm since it is difficult to check the orientation consistency between the multiple local surfaces contained in the same cell. The success of the proposed method is heavily dependent on the reconstruction results of the local implicit surfaces. It is especially difficult to correctly reconstruct topologically complex local regions without enough sample points and orientation information. Besides, it is also very difficult for a local method to distinguish between real surface samples and outliers. If local surfaces are not properly reconstructed, any orientation assignment does not make any sense and artifacts in the reconstructed surfaces are inevitable.

## VIII. CONCLUSION

We have presented an orientation inference framework for surface reconstruction from unorganized point clouds and demonstrated its effectiveness by showing the satisfactory reconstruction results from a variety of data sets. The proposed method can effectively reconstruct surfaces from both 3D scanned data sets and qualitatively inferior point clouds recovered from images. The basic idea of our method is to resolve the orientation of a set of unoriented local implicit surfaces, instead of discrete surface samples, through a graph optimization scheme. The proposed method is capable of generating multi-resolution models and repairing the reconstructed models under an unified progressive reconstruction framework. The proposed surface reconstruction algorithm was not developed to achieve the utmost efficiency, but we believe that it will benefit from modern graphics hardware to further improve its computational performance since much of the matrix computation required in the RBF fitting can be greatly accelerated by GPUs.

## REFERENCES

[1] M. Levoy, K. Pulli, B. Curless, S. Rusinkiewicz, D. Koller, L. Pereira, M. Ginzton, S. Anderson, J. Davis, J. Ginsberg, J. Shade, and D. Fulk, "The digital michelangelo project: 3d scanning of large statues," in *Proceedings of ACM SIGGRAPH '00*, 2000, pp. 131–144.

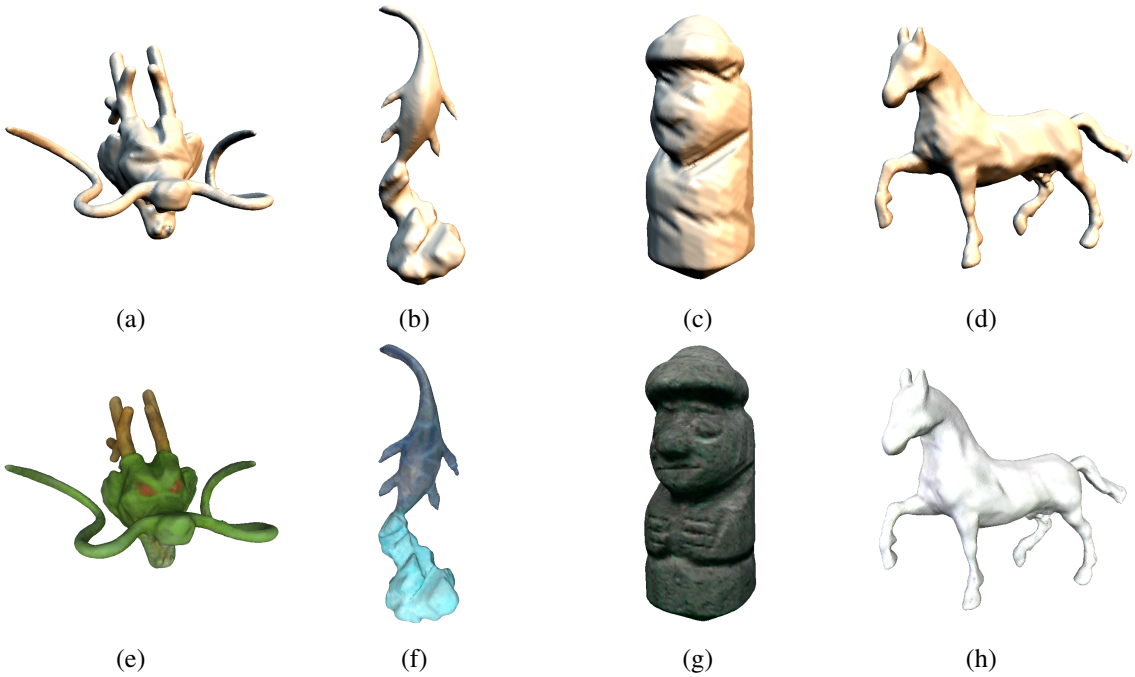


Fig. 16. (a)-(d): Reconstructed implicit surfaces by applying the proposed method with color mapping. to the image-based 3D reconstructed data sets. (e)-(f): Reconstructed surface models rendered with texture mapping.


[2] A. Robles-Kelly and E. R. Hancock, "A graph-spectral approach to shape-from-shading," *IEEE Transactions on Image Processing*, vol. 13, no. 7, pp. 912–926, July 2004.

[3] O. Faugeras and R. Keriven, "Variational principles, surface evolution, pdes, level set methods, and the stereo problem," *IEEE Transactions on Image Processing*, vol. 7, no. 3, pp. 336–344, March 1998.

[4] W. L. Hwang, C.-S. Lu, and P.-C. Chung, "Shape from texture: Estimation of planar surface orientation through the ridge surfaces of continuous wavelet transform," *IEEE Transactions on Image Processing*, vol. 7, no. 5, pp. 773–780, May 1998.

[5] G. Atkinson and E. R. Hancock, "Recovery of surface orientation from diffuse polarization," *IEEE Transactions on Image Processing*, vol. 15, no. 6, pp. 1653–1664, June 2006.

[6] D. Shin and T. Tjahjadi, "Local hull-based surface construction of volumetric data from silhouettes," *IEEE Transactions on Image Processing*, vol. 17, no. 8, pp. 1251–1260, August 2008.

[7] B. D. Rigling and R. L. Moses, "Three-dimensional surface reconstruction from multistatic sar images," *IEEE Transactions on Image Processing*, vol. 14, no. 8, pp. 1159–1171, August 2005.

[8] P.-H. Huang and S.-H. Lai, "Contour-based structure from reflection," in *Proceedings of IEEE Conference on Computer Vision and Pattern Recognition (CVPR'06)*, 2006, pp. 379–386.

[9] M. Alexa, J. Behr, D. Cohen-Or, S. Fleishman, D. Levin, and C. T. Silva, "Point set surfaces," in *Proceedings of IEEE Visualization '01*, October 2001, pp. 21–28.

[10] N. Amenta and Y. J. Kil, "Defining point-set surfaces," *ACM Transactions on Graphics (Proceedings of ACM SIGGRAPH '04)*, vol. 23, no. 3, pp. 264–270, 2004.

[11] J.-D. Boissonnat and F. Cazals, "Smooth surface reconstruction via natural neighbour interpolation of distance functions," in *Proceedings of annual symposium on Computational geometry*, 2000, pp. 223–232.

[12] T. K. Dey and J. Sun, "An adaptive mls surface for reconstruction with guarantees," in *SGP'05: Proceedings of Eurographics Symposium on Geometry processing*, 2005, p. 43.

[13] H. Hoppe, T. DeRose, T. Duchamp, J. McDonald, and W. Stuetzle, "Surface reconstruction from unorganized points," in *Proceedings of ACM SIGGRAPH '92*, July 1992, pp. 71–78.

[14] H. Xie, J. Wang, J. Hua, H. Qin, and A. Kaufman, "Piecewise c1 continuous surface reconstruction of noisy point clouds via local implicit quadric regression," in *Proceedings of IEEE Visualization '03*, 2003, pp. 91–98.

[15] G. Guennebaud and M. Gross, "Algebraic point set surfaces," *ACM Transactions on Graphics (Proceedings of ACM SIGGRAPH '07)*, vol. 26, no. 3, pp. 23:1–23:8, 2007.

[16] M. Pauly, R. Keiser, L. Kobbelt, and M. Gross, "Shape modeling with point-sampled geometry," *ACM Transactions on Graphics (Proceedings of ACM SIGGRAPH '03)*, vol. 22, no. 3, pp. 641–650, 2003.

[17] H. Huang, D. Li, H. Zhang, U. Ascher, and D. Cohen-Or, "Consolidation of unorganized point clouds for surface reconstruction," *ACM Transactions on Graphics (Proceedings of ACM SIGGRAPH Asia '09)*, vol. 28, no. 5, pp. 176:1–176:7, 2009.

[18] D. Marr and T. Poggio, "Cooperative computation of stereo disparity," *Science*, vol. 194, no. 4262, pp. 283–287, October 1976.

[19] J. Pearl, *Probabilistic Reasoning in Intelligent Systems: Networks of Plausible Inference*. San Mateo, California: Morgan Kaufmann, 1988.

[20] Y. Ohtake, A. Belyaev, M. Alexa, G. Turk, and H.-P. Seidel, "Multi-level partition of unity implicits," in *Proc. of ACM SIGGRAPH '03*, July 2003, pp. 463–470.

[21] I. Tobor, P. Reuter, and C. Schlick, "Multi-scale reconstruction of implicit surfaces with attributes from large unorganized point sets," in *Proceedings of Shape Modeling International '04*, 2004, pp. 19–30.

[22] J. P. Gois, V. Polizelli-Junior, T. Etiene, E. Tejada, A. Castelo, L. G. Nonato, and T. Ertl, "Twofold adaptive partition of unity implicits," *The Visual Computer*, vol. 24, no. 12, pp. 1013–1023, 2008.

[23] Y. Ohtake, A. G. Belyaev, and H.-P. Seidel, "A multi-scale approach to 3d scattered data interpolation with compactly supported basis functions," in *Shape Modeling International '03*, May 2003, pp. 153–161.

[24] G. Turk and J. F. O'Brien, "Modelling with implicit surfaces that interpolate," *ACM Transactions on Graphics*, vol. 21, no. 4, pp. 855–873, October 2002.

[25] H. Edelsbrunner and E. P. Mücke, "Three-dimensional alpha shapes," *ACM Transactions on Graphics*, vol. 13, no. 1, pp. 43–72, 1994.

[26] N. Amenta, S. Choi, and R. K. Kolluri, "The power crust," in *Proceedings of ACM symposium on Solid modeling and applications*, 2001, pp. 249–266.

[27] T. K. Dey and J. Giesen, "Detecting undersampling in surface reconstruction," in *SCG '01: Proceedings of Symposium on Computational geometry*, 2001, pp. 257–263.

[28] T. K. Dey, J. Giesen, and J. Hudson, "Delaunay based shape reconstruction from large data," in *Proceedings of IEEE Symposium on Parallel and Large Data Visualization*, 2001, pp. 19–27.

[29] F. Cazals and J. Giesen, "Delaunay triangulation based surface reconstruction," in *Effective Computational Geometry for Curves and Surfaces*. Springer, 2006.

[30] G. Taubin, "An improved algorithm for algebraic curve and surface

fitting," in *Proceedings of International Conference on Computer Vision (ICCV'93)*, May 1993, pp. 658–665.
[31] Y. Ohtake, A. Belyaev, and M. Alexa, "Sparse low-degree implicit surfaces with applications to high quality rendering, feature extraction, and smoothing," in *SGP'05: Proceedings of Eurographics Symposium on Geometry processing*, 2005, pp. 149:1–149:8.
[32] H.-K. Zhao, S. Osher, B. Merriman, and M. Kang, "Implicit and nonparametric shape reconstruction from unorganized data using a variational level set method," *Computer Vision Image Understanding*, vol. 80, no. 3, pp. 295–314, 2000.
[33] Y. Lipman, D. Cohen-Or, and D. Levin, "Data-dependent mls for faithful surface approximation," in *SGP'07: Proceedings of the fifth Eurographics symposium on Geometry processing*, 2007, pp. 59–67.
[34] S. Fleishman, D. Cohen-Or, and C. T. Silva, "Robust moving least-squares fitting with sharp features," *ACM Transactions on Graphics (Proceedings of ACM SIGGRAPH'05)*, vol. 24, no. 3, pp. 544–552, 2005.
[35] R. Kolluri, "Provably good moving least squares," in *SIGGRAPH '05: ACM SIGGRAPH 2005 Courses*, 2005, p. 213.
[36] J. C. Carr, R. K. Beatson, J. B. Cherrie, T. J. Mitchell, W. R. Fright, B. C. McCallum, and T. R. Evans, "Reconstruction and representation of 3d objects with radial basis functions," in *Proceedings of ACM SIGGRAPH '01*, August 2001, pp. 67–76.
[37] H. Q. Dinh, G. Turk, and G. Slabaugh, "Reconstructing surfaces by volumetric regularization using radial basis functions," *IEEE Transactions on Pattern Analysis and Machine Intelligence*, vol. 24, no. 10, pp. 1358–1371, October 2002.
[38] M. Kazhdan, M. Bolitho, and H. Hoppe, "Poisson surface reconstruction," in *Proc. of Eurographics Symposium on Geometry Processing*, 2006, pp. 61–70.
[39] P. Alliez, D. Cohen-Steiner, Y. Tong, and M. Desbrun, "Voronoi-based variational reconstruction for unoriented point sets," in *Proceedings of Eurographics Symposium on Geometry Processing*, 2007, pp. 39–48.
[40] H. Xie, K. T. McDonnel, and H. Qin, "Surface reconstruction of noisy and defective data sets," in *Proceedings of IEEE Visualization '04*, 2004, pp. 259–266.
[41] N. Amenta, M. Bern, and M. Kamvysselis, "A new voronoi-based surface reconstruction algorithm," in *Proceedings of ACM SIGGRAPH '98*, August 1998, pp. 415–420.
[42] N. Amenta and M. Bern, "Surface reconstruction by voronoi filtering," *Geometry: Discrete and Computational Geometry*, vol. 22, 1999.
[43] N. J. Mitra, A. Nguyen, and L. Guibas, "Estimating surface normals in noisy point cloud data," in *International Journal of Computational Geometry and Applications*, vol. 14, no. 4–5, 2004, pp. 261–276.
[44] T. K. Dey, G. Li, and J. Sun, "Normal estimation for point clouds: a comparison study for a voronoi based method," in *Proceedings of Symposium on Point-Based Graphics*, 2005, pp. 39–46.

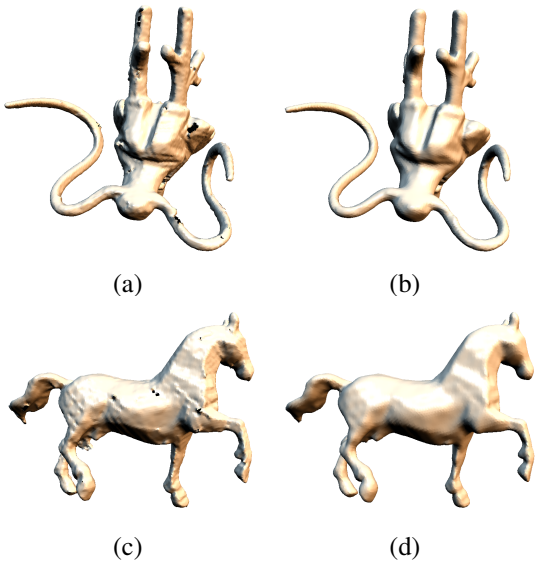


Fig. 15. Reconstructed surfaces from the DRAGON and HORSE data sets by (a)(c) algebraic point set surfaces [15], and (b)(d) the proposed method, respectively.

[45] D. OuYang and H.-Y. Feng, "On the normal vector estimation for point cloud data from smooth surfaces," *Computer-Aided Design*, vol. 37, no. 10, pp. 1071–1079, 2005.
[46] Y. Lipman, D. Cohen-Or, D. Levin, and H. Tal-Ezer, "Parameterization-free projection for geometry reconstruction," *ACM Transactions on Graphics (Proceedings of ACM SIGGRAPH '07)*, vol. 26, no. 3, p. 22, 2007.
[47] A. C. Jalba and J. B. T. M. Roerdink, "Efficient surface reconstruction from noisy data using regularized membrane potentials," *IEEE Transactions on Image Processing*, vol. 18, no. 5, pp. 1119–1134, May 2009.
[48] Y. Boykov, O. Veksler, and R. Zabih, "Fast approximate energy minimization via graph cuts," *IEEE Transactions on Pattern Analysis and Machine Intelligence*, vol. 23, no. 11, pp. 1222–1239, November 2001.
[49] Y. Weiss and W. T. Freeman, "On the optimality of solutions of the max-product belief propagation algorithm in arbitrary graphs," *IEEE Transactions on Information Theory*, vol. 47, no. 2, pp. 723–735, 2001.
[50] B. S. Morse, T. S. Yoo, P. Rheingans, D. T. Chen, and K. R. Subramanian, "Interpolating implicit surfaces from scattered data using compactly supported radial basis functions," in *Shape Modeling International '01*, May 2001, pp. 89–98.
[51] D. V. Ouellette, "Schur complements and statistics," *Linear Algebra and its Applications*, vol. 36, pp. 187–295, 1981.
[52] G. Turk and J. F. O'Brien, "Shape transformation using variational implicit surfaces," in *Proceedings of ACM SIGGRAPH '99*, August 1999, pp. 335–342.
[53] M. Pauly, M. Gross, and L. P. Kobbelt, "Efficient simplification of point-sampled surfaces," in *Proceedings of IEEE Visualization '02*, October 2002, pp. 163–170.
[54] J. Sun, M. Smith, L. Smith, and A. Farooq, "Examining the uncertainty of the recovered surface normal in three light photometric stereo," *Image and Vision Computing*, vol. 25, no. 7, pp. 1073–1079, 2007.
[55] W.-C. Ma, T. Hawkins, P. Peers, C.-F. Chabert, M. Weiss, and P. Debevec, "Rapid acquisition of specular and diffuse normal maps from polarized spherical gradient illumination," in *Eurographics Symposium on Rendering 2007*, 2007, pp. 183–194.
[56] P. Cignoni, M. Corsini, and G. Ranzuglia, "Meshlab: an open-source 3d mesh processing system," *ERCIM News*, no. 73, pp. 45–46, April 2008. [Online]. Available: http://vcg.isti.cnr.it/Publications/2008/CCR08

**Yi-Ling Chen** received the B.S. and M.S. degrees in Computer Science from National Tsing Hua University, Hsinchu, Taiwan, R.O.C. in 2002 and 2004, respectively. He is pursuing his Ph.D degree in the same department since 2005. His research interests include computer vision and graphics, geometric modeling and processing, surface reconstruction.

**Shang-Hong Lai** (M'95-) received the B.S. and M.S. degrees in electrical engineering from National Tsing Hua University, Hsinchu, Taiwan, and the Ph.D. degree in electrical and computer engineering from University of Florida, Gainesville, in 1986, 1988 and 1995, respectively. He joined Siemens Corporate Research in Princeton, New Jersey, as a member of technical staff in 1995. Since 1999, he became a faculty member in the Department of Computer Science, National Tsing Hua University, Taiwan. He is currently a professor in the same department. In 2004, he was a visiting scholar with Princeton University. Dr. Lai's research interests include computer vision, visual computing, pattern recognition, medical imaging, and multimedia signal processing. He has authored more than 150 papers published in the related international journals and conferences. He holds many patents for inventions related to computer vision and medical image analysis. He has been a member of program committee of several international conferences, including CVPR, ICCV, ECCV, ACCV, ICPR and ICME.